A Weak Target Detection Algorithm IAR-STFT Based on Correlated K-distribution Sea Clutter Model

Yaowen LIU [1], Xuan RAO [1], Jianfen HU [1], Xiangsheng ZHU [1, 2], Hong YI [1]

[1] Nanchang Hangkong University, 696 South Fenhe Avenue, 330063 Nanchang, China
[2] North Alliance Communication Company, 168 Jingdong Avenue, High-tech Development Zone, 330063 Nanchang, China

985925536@qq.com, raoxuancom@163.com, 46044@nchu.edu.cn, zhuxs1993@163.com, hongyi_rsp2021@163.com

Submitted June 14, 2022 / Accepted November 3, 2022 / Online first December 16, 2022

Abstract. *The detection performance of weak target on sea is affected by the special effects of sea clutter amplitude. Aiming at the time and space correlated of sea clutter, the correlated K-distribution sea clutter model is established by the sphere invariant random process algorithm. To solve the problems of range migration (RM) and Doppler frequency migration (DFM) of moving target in the case of long-time coherent accumulation, a novel integration detection algorithm, improved axis rotation short-time Fourier transform (IAR-STFT) is proposed in this paper, which is based on a generalization of traditional Fourier transform (FT) algorithm and combined with improved axis rotation. IAR-STFT not only can eliminate the RM effect by searching for the target motion parameters, but also can divide the non-stationary echo signal without range migration into several blocks. Each block of signal can be regarded as a stationary signal without DFM and FFT is performed on each signal separately. The signals of each block are accumulated to detect the target in the background of the above sea clutter. Finally, the effectiveness of the algorithm is verified by simulation. The results show that the detection ability of this algorithm is better than that of Radon-fractional Fourier transform, generalized Radon Fourier transform and Radon-Lv's distribution in low SNR environment, e.g., when the SNR is –45 dB, the detection ability of this algorithm is about 55%, which is higher than that of Radon-fractional Fourier transform, generalized Radon Fourier transform and Radon-Lv's distribution.*

Keywords

Correlated K-distribution, range migration, Doppler frequency migration, long time coherent accumulation, improved axis rotation short-time Fourier transform

RM	Range Migration
DFM	Doppler Frequency Migration
IAR	Improved Axis Rotation
STFT	Short-Time Fourier Transform
FT	Fourier Transform
FFT	Fast Fourier Transform
LVD	LV's Distribution
RLVD	Radon-LV's Distribution
SCR	Signal to Clutter Ratio
RCS	Radar Cross Section
DBT	Detection Before Tracking
TBD	Tracking Before Detection
RFT	Radon-Fourier Transform
FRFT	FRactional Fourier Transform
RFRFT	Radon-FRactional Fourier Transform
GRFT	Generalized Radon-Fourier Transform
CFAR	Constant False Alarm Rate
PDF	Probability Density Function
ZMNL	Zero-Memory NonLinear
SIRP	Spherical Invariant Random Process
WDR	Ratio of Window width to each Delay
IAR-STFT	Improved Axis Rotation Short-Time Fourier Transform
IAR-FRFT	Improved Axis Rotation FRactional Fourier Transform

Tab. 1. Table of abbreviations.

1. Introduction

In general, the influence of sea clutter is huge when detecting sea surface targets. To detect the targets accurately, sea clutter must be suppressed. The environment is very complex because of various factors on the sea surface. Environment: such as the wind speed, wind direction, wave height and temperature of the sea surface; and the different working conditions of the radar such as: incident angle, signal transmission frequency, polarization mode and resolution, etc., will affect the detection performance [1]. The

DOI: 10.13164/re.2023.0033

establishment of the sea clutter model is of great significance for the statistical analysis of sea clutter [2]. Recently, many scholars have mainly studied two aspects of sea clutter: The first is to describe the changes in the structure of the sea clutter simulation mathematical model [3]; the second is to study the sea clutter simulation algorithm to simulate the dynamic characteristics of sea clutter [4]. However, since the correlated K distribution is more suitable to describe the correlated characteristics of sea clutter, the mechanism can be explained well [5].

Radar is widely used for target detection and tracking. It is very important to detect moving targets in strong sea clutter, whether in the military field or civil field [6], [7]. The complexity of target detection is not only related to target motion parameters, but also affected by the clutter background and radar parameters in the marine environment. There are many kinds of weak moving targets, which can usually be summarized as "long-distance, low observable, and high maneuvering" targets, and radar cross section (RCS) of maneuvering target is usually very small, which reduces the output signal to clutter ratio (SCR) and detection performance of radar [8], [9]. With the occurrence of the above situations, the application of modern radar has put forward higher requirements. It is well-known that the detection performance and SCR of radar returns can be improved significantly by long-time accumulation [9–11].

When high-resolution radar is used to detect weak targets in strong clutter background, the energy of radar echo signal is weak due to the small RCS, which makes it difficult to detect and track weak targets by using traditional detection before tracking (DBT) technology. The energy accumulation of echo can be improved by using tracking before detection (TBD) technology to increase the coherent accumulation time of echo, Thus, the performance of weak target detection and tracking is improved effectively [12], [13].

When radar detects high speed and constant acceleration targets under strong sea clutter background, range migration (RM) and Doppler frequency migration (DFM) will occur within a long coherent accumulation time [14–16]. The influence of RM on coherent integration can be eliminated by standard Radon-Fourier transform (RFT) [17] and IAR algorithm [10]. FRFT can eliminate the influence of DFM on coherent integration by choosing a suitable transformation order [18]. The Radon-fractional Fourier transform (RFRFT) is proposed based on radon transform and fractional Fourier transform. The RFRFT not only can eliminate RM by radon transform but also achieve long-time coherent accumulation via FRFT for the maneuvering targets in low SCR [9, 14, 19]. A new weak maneuvering target detection method in a sea environment with a Radon-fractional Fourier transform (RFRFT) canceller is proposed in [20], which can efficiently suppress the sea clutter and detect targets with low computations. Similarly, an algorithm improved axis rotation FRFT (IAR-FRFT) is proposed to eliminate RM via IAR transform and the echo signal is coherent accumulated via FRFT [20].

To eliminate high-order RM and DFM, the generalized RFT (GRFT) algorithm is proposed in [22], [23]. GRFT searches for the initial radial distance, velocity and acceleration of each order, compensates the phase terms of the parameters searched above, and accumulates the echoes. GRFT does not need to consider the effect of RM and DFM on coherent integration. However, the multidimensional search of GRFT and the compensation of higher-order motion parameters bring huge computational complexity [24].

Based on the research of RFT and Lv's distribution (LVD) [25], another algorithm, RLVD, for weak target detection with complex motion is proposed. Compared with GRFT, RLVD, RFRFT and IAR-FRFT, it not only can eliminate the influence of RM and DFM during coherent accumulation, but also improve the output SCR of the signal under the same input SCR to RLVD can achieve better signal accumulation and detection performance in the CFAR domain without requiring more computational costs [26–28].

RM and DFM increase not only with the increase of velocity and acceleration, but also with the increase of coherent accumulation time [8], [14]. Because the velocity and acceleration are unknown, to reduce RM and DFM, only the coherent accumulation time can be considered to change. But the reduction of the coherent accumulation time will affect the energy accumulation effect of the weak target. To reduce the influence of RM and DFM while keeping the coherent accumulation time unchanged, a novel detection algorithm improved axis rotation short-time Fourier transform (IAR-STFT) is proposed in this paper. By using the improved axis rotation transform, the echoes signal obtained keeps in a same range cell during the long coherent accumulation time [29], [30]. Then the echoes are divided into several sections by using a moving window. The echoes can be regarded as stationary in each short time slice. Therefore, DFM can be ignored in each time slice and the signal can be accumulated effectively via FFT [31] in a very short time. Choosing a suitable width of window to achieve high resolution in both the time and frequency (2-D resolution) [32], [33]. Simulation results show the accumulation effect of IAR-STFT is better than that of GRFT, RFRFT, IAR-FRFT, RLVD. IAR-STFT requiring the computational complexity is lower. The main contributions of this article are:

1) According to the maximum 2-D resolution and the better time-frequency aggregation, provide a selecting optimal window function method based on the uncertainty principle.

2) The proposed algorithm IAR-STFT can accumulate the target's echoes with RM and DFM effectively instead of FT.

3) Adjust the window delay to improve the detection performance of IAR-STFT according to different SCR environments.

The rest is organized as follows. The clutter model and signal model are introduced in Sec. 2. Then, in Sec. 3, IAR-STFT is proposed and analyzed. In Sec. 4 and Sec. 5, the effectiveness of the algorithm is verified by numerical experiments and the conclusion is given respectively.

2. Clutter Model and Signal Model

2.1 Clutter Model

According to the central limit theorem, most of the clutter models belong to Gaussian distribution. For high-resolution radar systems, the sea clutter model has a large tail delay, which makes the traditional Gaussian clutter model being inconsistent with the actual sea clutter. Thus, various non-Gaussian probability distributions, e.g., log-normal distribution, Weibull distribution and correlated K distribution model, are consistent with the actual sea clutter [34], [35]. Considering that sea clutter has both time and space correlated, so the correlated K distribution is more useful.

Probability density function (PDF) of correlated K distribution is given as

$$f(x)=\frac{2}{\alpha\Gamma(\nu)}\left(\frac{x}{2\alpha}\right)^{\nu}K_{\nu-1}\left(\frac{x}{\alpha}\right),\alpha>0,\nu>0,x>0 \quad (1)$$

where α is the scale parameter; $\Gamma(\nu)$ is the Gamma function; ν is the shape parameter whose value range is $(0.1, \infty)$. When $\nu\to 0.1$, clutter has a large tail delay and when $\nu\to\infty$, the distribution will be close to Rayleigh. For sea clutter with high resolution and low grazing angle, the value of ν is (0.1, 3). $K_{\nu}(\cdot)$ is the second kind of modified Bessel function of order ν.

Performing a series of transforms on the Gaussian sequence to obtain the non-Gaussian sequence is a key for sea clutter modeling. The algorithms of simulating sea clutter mainly include the zero-memory nonlinear transformation (ZMNL) algorithm and the spherical invariant random process (SIRP) algorithm [4], [34]. SIRP can independently control the auto correlated of edge PDF and clutter, which overcomes the influence of ZMNL on auto correlated. In this paper, the SIRP algorithm is used to establish a correlated K-distribution sea clutter. The one-dimensional generation process of the sea clutter correlated K-distribution sequence is proposed in [35], and here we give the two-dimensional generation process composition block diagram of sea clutter related K-distribution sequence, as shown in Fig. 1.

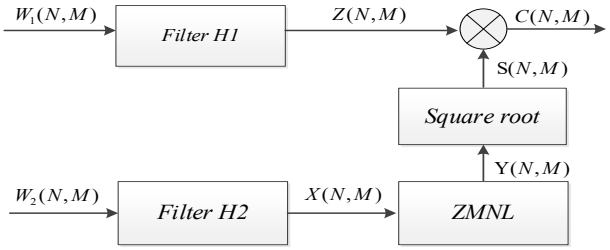

Fig. 1. The generation process composition block diagram of sea clutter with correlated K distribution.

$W_1(N,M)$ is a randomly generated complex Gaussian white noise matrix. Linear filter H1 is determined by the output clutter data matrix $C(N,M)$. $W_2(N,M)$ is a random Gaussian white noise matrix, and filter H2 is a low-pass digital filter. The matrix $X(N,M)$ is subjected to zero-memory nonlinear transformation (ZMNT) to obtain the related gamma distribution matrix $Y(N,M)$, and then takes the square root of the $Y(N,M)$ to obtain the chi distribution matrix $S(N,M)$. Finally, the corresponding elements of $S(N,M)$ and $Z(N,M)$ are multiplied to obtain two-dimensional sea clutter data $C(N,M)$, where N is the sampling number of fast time and M is that of slow time.

2.2 Signal Model

Assume that the motion model of a moving target is given as follows

$$R(t_m)=R_0+vt_m+\frac{1}{2}at_m^2, t_m\in[0,T] \quad (2)$$

where R_0 is the initial slant range, v is the radial velocity and a is the radial acceleration of the target respectively, $t_m=mT_r(m=1,2,3,\ldots,M)$ is the slow time between the pulse and the pulse, m is the number of pulses, T_r is the pulse repetition interval, T is the coherent accumulation time.

Suppose that the linear frequency modulation (LFM) signal transmitted by the radar after modulation is

$$s(t)=\mathrm{rect}\left(\frac{t}{T_p}\right)\exp(\mathrm{j}\pi kt^2)\exp(\mathrm{j}2\pi f_c t) \quad (3)$$

where $\mathrm{rect}\left(\frac{t}{T_p}\right)=\begin{cases}1, \left|\frac{t}{T_p}\right|\le\frac{1}{2}\\ 0, \left|\frac{t}{T_p}\right|\le\frac{1}{2}\end{cases}$, T_p is the width of the pulse, f_c is the carrier frequency, k is the frequency modulated rate, and let $t=\hat{t}+t_m$, where $\hat{t}$ is the electromagnetic transmission time called fast time.

The received baseband echo after demodulation and pulse compression can be expressed as

$$s_{\mathrm{pc}}(\hat{t},t_m)=A\,\mathrm{sinc}\left(B\left(\hat{t}-\frac{2R(t_m)}{c}\right)\right)\times\exp\left(-\mathrm{j}\frac{4\pi f_{\mathrm{c}}R(t_m)}{c}\right) \tag{4}$$

where A is the amplitude of signal after pulse compression, B is the bandwidth of transmission signal, and c is the speed of light.

It can be seen from (2) and (4) that the envelope of echoes will change with the slow time. During the long-time coherent accumulation, the range change will exceed a range resolution, i.e., $\rho = c/(2B)$, and the RM effect would occur. The phase term also has a quadratic term which changes with slow time due to acceleration, which will lead to DFM and make the energy not concentrated [14]. IAR-STFT can eliminate RM and DFM during long time coherent accumulation.

3. Principle of IAR-STFT

The most of the signals received by radar are non-stationary signals [36], while FFT can only deal with stationary signals, which limit its applications in target detection and echoes analysis. Therefore, a novel algorithm IAR-STFT is proposed, which adopts sliding window to segment non-stationary signals [37] to keep each segment data be stationary and then performs FT. The process of IAR-STFT processing is shown in Fig. 2.

In Fig. 2, the transform of IAR delete the RM of echoes, the IAR relationship is given as follows, where α is the axis rotation angle.

$$\begin{cases} m=m' \\ n_{\mathrm{r}}=\mathrm{round}\left(m'\tan\alpha+n'_{\mathrm{r}}\dfrac{1}{\cos\alpha}\right). \\ \alpha\in\left(-\dfrac{\pi}{2},\dfrac{\pi}{2}\right) \end{cases} \tag{5}$$

IAR-STFT combines the algorithms with time domain analysis and frequency domain analysis which not only

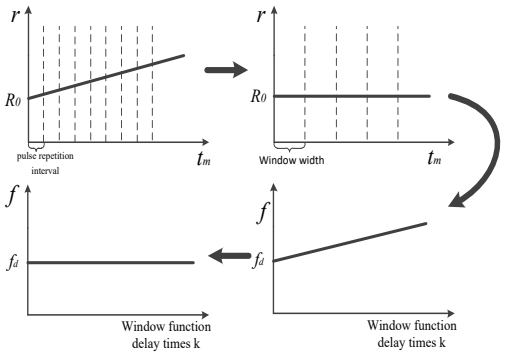

Fig. 2. Process of IAR-STFT.

reflects the frequency component, but also reflects the change rule of the frequency component changing with the delay of window. STFT [38], [39] of a signal $x(t)$ is defined as

$$STFT_{\mathrm{x}}(\tau,f)=\int_{-\infty}^{+\infty}x(t)g(t-\tau)\exp(-\mathrm{j}2\pi ft)\,\mathrm{d}t \tag{6}$$

where τ is delay of the window function. To obtain the best time-frequency resolution, Gaussian window should be adopted [40].

3.1 Selection of Window

IAR-STFT algorithm is used to eliminate DFM caused by the acceleration in each window. According to the uncertainty principle, the relationship between time resolution and frequency resolution is inversely. The narrower the window is, the higher the time resolution is; a wider window may help improve frequency resolution but the time resolution will decrease [41]. To obtain higher time-frequency resolution, Gauss function is defined as

$$g(t)=\frac{1}{\sqrt{2\pi}\sigma}\mathrm{e}^{-\frac{t^2}{2\sigma^2}} \tag{7}$$

where σ is the standard deviation of Gaussian function, the FFT of $g(t)$ may be rewritten as

$$G(f)=\mathrm{e}^{2\pi^2\sigma^2f^2}. \tag{8}$$

The mean value of time domain and mean value of frequency of the function are defined as

$$t_0=\frac{\int_{-\infty}^{+\infty}t\left|g(t)\right|^2\mathrm{d}t}{\int_{-\infty}^{+\infty}\left|g(t)\right|^2\mathrm{d}t}=0, \tag{9}$$

$$f_0=\frac{\int_{-\infty}^{+\infty}f\left|G(f)\right|^2\mathrm{d}f}{\int_{-\infty}^{+\infty}\left|G(f)\right|^2\mathrm{d}f}=0. \tag{10}$$

They are squared time-width and squared frequency-bandwidth of the function are defined as [42]

$$(\Delta t)^2=\frac{\int_{-\infty}^{+\infty}(t-t_0)^2\left|g(t)\right|^2\mathrm{d}t}{\int_{-\infty}^{+\infty}\left|g(t)\right|^2\mathrm{d}t}=\frac{\sigma^2}{2}, \tag{11}$$

$$(\Delta f)^2=\frac{\int_{-\infty}^{+\infty}(f-f_0)^2\left|G(f)\right|^2\mathrm{d}f}{\int_{-\infty}^{+\infty}\left|G(f)\right|^2\mathrm{d}f}=\frac{1}{8\pi^2\sigma^2}. \tag{12}$$

The time-frequency-bandwidth product (TBP) of the Gaussian function is

$$\Delta t\Delta f=\frac{1}{4\pi}. \tag{13}$$

Gauss window function can satisfy the inequality of uncertainty principle to take equal sign, and it is found that Gaussian window function can obtain high two-dimensional resolution and time-frequency aggregation which is better.

3.2 Introduction of IAR-STFT

The relationship between the fast time $\hat{t}$ and the distance range r is $\hat{t} = 2r/c$. Then (4) may be rewritten as

$$s_{\mathrm{pc}}(r,t_m)=A\,\mathrm{sinc}\left(\frac{2B}{c}\left(r-(R_0+vt_m+\frac{1}{2}at_m^2)\right)\right)\times\exp\left(-\mathrm{j}\frac{4\pi}{\lambda}(R_0+vt_m+\frac{1}{2}at_m^2)\right). \tag{14}$$

The number of distance cell corresponding to r is $n_{\mathrm{r}} = r/\rho = (2B/c)r$, and the number of distance cell R_0 is $n_{\mathrm{R}_0} = R_0/\rho = (2B/c)R_0$, respectively. The effect of acceleration on RM of echo can be ignored, then (14) is given as

$$s_{\mathrm{pc}}(n_{\mathrm{r}},m)=A\,\mathrm{sinc}\left(n_{\mathrm{r}}-n_{\mathrm{R}_0}-\frac{vmT_{\mathrm{r}}}{\rho}\right)\exp\left(-\mathrm{j}\frac{4\pi}{\lambda}n_{\mathrm{R}_0}\rho\right)\times\exp\left(-\mathrm{j}\frac{4\pi}{\lambda}vmT_{\mathrm{r}}\right)\exp\left(-\mathrm{j}\frac{4\pi}{\lambda}\frac{1}{2}a(mT_{\mathrm{r}})^2\right). \tag{15}$$

Substituting (5) into (15) yields

$$s_{\mathrm{pc}}(n_{\mathrm{r}}',m')=A\,\mathrm{sinc}\left(\frac{1}{\cos\alpha}(n_{\mathrm{r}}'-n_{\mathrm{R}_0}\cos\alpha)\right)\exp\left(-\mathrm{j}\frac{4\pi}{\lambda}n_{\mathrm{R}_0}\rho\right)\times\exp\left(-\mathrm{j}\frac{4\pi}{\lambda}vm'T_{\mathrm{r}}\right)\exp\left(-\mathrm{j}\frac{4\pi}{\lambda}\frac{1}{2}a(m'T_{\mathrm{r}})^2\right). \tag{16}$$

In the new coordinate system ($n_{\mathrm{r}}'-m'$), the echo envelope amplitude is distributed in the range cell $n_{\mathrm{r}_0}' = n_{\mathrm{R}_0}\cos\alpha$. The distance range $r' = n_{\mathrm{r}}'\times\rho = c/(2B)n_{\mathrm{r}}'$, $n_{\mathrm{r}_0}' = n_{\mathrm{R}_0}'\cos\alpha = (2B/c)R_0\cos\alpha$, slow time $t_m' = m'T_{\mathrm{r}}$, then (16) may be rewritten as

$$s_{\mathrm{pc}}(r',t_m')=A\,\mathrm{sinc}\left(\frac{2B}{c\cos\alpha}(r'-R_0\cos\alpha)\right)\exp\left(-\mathrm{j}\frac{4\pi}{\lambda}R_0\right)\times\exp\left(-\mathrm{j}\frac{4\pi}{\lambda}vt_m'\right)\exp\left(-\mathrm{j}\frac{4\pi}{\lambda}\frac{1}{2}at_m'^2\right). \tag{17}$$

Then taking (17) into the definition (6) of STFT yields

$$\begin{aligned}STFT_{s_{\mathrm{pc}}}(r',f,\tau)&=\int_{-\infty}^{+\infty}s_{\mathrm{pc}}(r',t_m')g(t_m'-\tau)\times\exp(-\mathrm{j}2\pi ft_m')\,\mathrm{d}t_m'\\&=\frac{1}{\sqrt{2\pi}\sigma}A\,\mathrm{sinc}\left(\frac{2B}{c\cos\alpha}(r'-R_0\cos\alpha)\right)\times\sqrt{\frac{\lambda}{8a}}\exp\left(-\frac{\left(\frac{\lambda}{2a}\right)^2}{2\sigma^2}\right)\\&\times\exp\left[-\frac{\left(f-\left(-\frac{2v_0+2a\tau}{\lambda}\right)\right)^2}{2\sigma^2}\right]\times\exp\left[\mathrm{j}\left(\frac{\pi\lambda f^2}{2a}+\frac{2\pi v_0 f}{a}+\frac{2\pi v_0^2}{\lambda a}\right)\right]\\&\times\exp\left[\mathrm{j}\left(-\frac{4\pi R_0}{\lambda}-\frac{\pi}{4}\right)\right].\end{aligned} \tag{18}$$

It can be seen from (18) that the envelope trajectory of the echo signal in the time-frequency domain plane after STFT is $f = -(2v_0 + 2a\tau)/\lambda = f_{\mathrm{d}0} + k_{\mathrm{d}}\tau$, where $f_{\mathrm{d}0}$ is the initial Doppler frequency and k_{d} is the Doppler modulation frequency. The phase corresponding to envelope trajectory is given as

$$\begin{aligned}\varphi(\tau)&=\frac{\pi\lambda f^2}{2a}+\frac{2\pi v_0 f}{a}+\frac{2\pi v_0^2}{\lambda a}-\frac{4\pi R_0}{\lambda}-\frac{\pi}{4}\\&=\pi k_{\mathrm{d}}\tau^2+4\pi f_{\mathrm{d}0}\tau+\frac{4\pi f_{\mathrm{d}0}^2}{k_{\mathrm{d}}}-\frac{4\pi R_0}{\lambda}-\frac{\pi}{4}.\end{aligned} \tag{19}$$

Analyzing the signal in a certain distance cell $r' = R_0\cos\alpha$ in (17), (18) may be rewritten as

$$STFT_{s_{\mathrm{pc}}}(f,\tau)=A'\exp\left[-\frac{\left(f-f_{\mathrm{d}0}-k_{\mathrm{d}}\tau\right)^2}{2\sigma^2}\right]\times\exp\left[\mathrm{j}\left(\pi k_{\mathrm{d}}\tau^2+4\pi f_{\mathrm{d}0}\tau+\frac{4\pi f_{\mathrm{d}0}^2}{k_{\mathrm{d}}}\right)\right]\times\exp\left[\mathrm{j}\left(-\frac{4\pi R_0}{\lambda}-\frac{\pi}{4}\right)\right] \tag{20}$$

where A' is

$$A' = \frac{A}{\sqrt{2\pi\sigma}} \operatorname{sinc}\left(\frac{2B}{c\cos\alpha}(r' - R_0\cos\alpha) \right) \times \exp\left(-\frac{\left(\frac{\lambda}{2a}\right)^2}{2\sigma^2} \right) \sqrt{\frac{\lambda}{8a}}.$$

From (20), it can be seen that there is a quadratic relationship between phase and window step τ, where $\tau = k \cdot LT_r/n$ (n = 1,2,3,…), and k is the number of moving times of the window function. To eliminate the influence of the quadratic term on energy accumulation, a phase compensation function is constructed as

$$h(\tau) = \exp(-\mathrm{j}\pi k_d \tau^2). \tag{21}$$

Multiply (20) by (21) and the quadratic term in the phase term of $\varphi(\tau)$ can be compensated. Then (20) may be rewritten as

$$STFT'_{s_{pc}}(f,\tau) = A' \exp\left[-\frac{(f - f_{d0} - k_d\tau)^2}{2\sigma^2} \right] \times \exp\left[\mathrm{j}\left(4\pi f_{d0}\tau + \frac{4\pi {f_{d0}}^2}{k_d} \right) \right] \times \exp\left[\mathrm{j}\left(-\frac{4\pi R_0}{\lambda} - \frac{\pi}{4} \right) \right]. \tag{22}$$

The IAR relationship in (5) may be rewritten as

$$\begin{cases} \tau = \tau' \\ f = \tau' \tan\alpha + f' \dfrac{1}{\cos\alpha} \end{cases}, \alpha \in \left(-\frac{\pi}{2}, \frac{\pi}{2} \right). \tag{23}$$

Substituting (23) into (22),

$$STFT'_{s_{pc}}(f',\tau') = A' \exp\left[\mathrm{j}\left(4\pi f_{d0}\tau' + \frac{4\pi {f_{d0}}^2}{k_d} \right) \right] \times \exp\left\{ -\frac{\left[\frac{1}{\cos\alpha}(f' - f_d\cos\alpha) \right]^2}{2\sigma^2} \right\} \times \exp\left[\mathrm{j}\left(-\frac{4\pi R_0}{\lambda} - \frac{\pi}{4} \right) \right]. \tag{24}$$

It is shown from (24) that signal amplitude envelope have been concentrated in the frequency cell $f' = f_d \cos\alpha$, improved axis rotation transform is adopted again to delete DFM in time-frequency field. The coherent integration result is obtained by FFT lastly. The process composition block diagram of the proposed accumulation algorithm based on IAR-STFT can be described in Fig. 3.

Carrier frequency	10 GHz
Bandwidth	25 MHz
Sample frequency	25 MHz
Pulse repetition frequency	6 KHz
Pulse duration	4 μs
Coherent integration time	0.2 s
Pulse number	1200

Tab. 2. Simulation parameters of radar.

4. Simulation and Numerical Results

To verify and compare the performance of IAR-STFT, several simulations are given in this section. The simulation parameters are shown in Tab. 2.

4.1 Resolution of Different Window Widths

For different window widths, the time resolution and frequency resolution are different. Choosing an appropriate window width is a key to improve the detection ability. There are several time-frequency maps of STFT with different window widths in Fig. 4. Assuming acceleration a = 10 m/s^2 and four different window widths are selected to analyze the two-dimensional resolution of time-frequency plane. The ratio of window width to each delay (WDR) is n, where n equals 4.

When the window width is small, the frequency resolution is very low and the time resolution is very high in Fig. 4(a) and 4(b). With the window width increasing, the frequency resolution will increase and the time resolution will decrease accordingly. When the window width L = 128, the frequency resolution will be very high, but the time resolution will be very poor in Fig. 4(d). As shown in Fig. 4(a) to 4(d), the increase of window width will lead to the decrease of time resolution and the increase of frequency resolution. To obtain a better detection performance, the appropriate window width should be chosen to improve the two-dimensional resolution as much as possible.

4.2 Coherent Accumulation for Weak Target

To compare the performance of IAR-STFT, GRFT, RFRFT, IAR-FRFT and RLVD to detect weak targets under the background of strong sea clutter, the detection results of these algorithms are given in Fig. 5 and the motion parameters of the maneuvering target are listed in Tab. 3. Figures 5(a), (b), (c) show the accumulation results of RFRFT, IAR-FRFT and RLVD, respectively. It can be found that the target has been buried by strong sea clutter, and the target cannot be detected. Moreover, Figures 5(d), (e) show the accumulation results of GRFT and IAR-STFT, respectively. On the conditions of the same parameters, IAR-STFT and GRFT can detect targets in strong sea

clutter. And we can see that IAR-STFT has a much larger clutter margin than GRFT, which means that the better detection capability can be achieved.

4.3 Coherent Accumulation Detection Ability

To demonstrate that the detection performance of IAR-STFT is better than that of RFRFT, IAR-FRFT, RLVD and GRFT, in this simulation, sea clutter data is constructed based on correlated K-distribution model and which is obtained by SIRP. We combine a constant false alarm (CFAR) detector with four algorithms as corresponding detectors, and the false alarm ratio $P_{fa} = 10^{-6}$. SCR of the four detection algorithms are set from –50 dB to –25 dB. Monte-Carlo simulation experiments are performed 100 times in each SCR to verify the detection performance of these five algorithms. Figure 6 shows the detection probability of the five detectors versus different SCRS. It can be found clearly that the performance of the proposed detector is much better than that of the other detectors. It also has a good performance in signal accumulation.

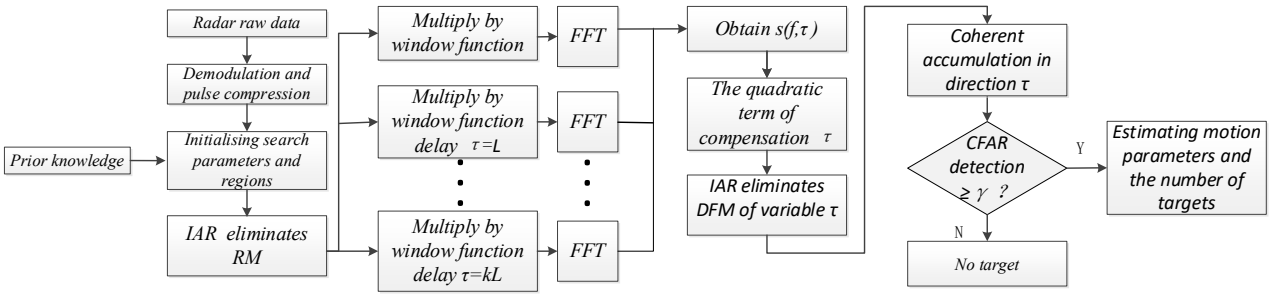

Fig. 3. Process composition block diagram of the long-time coherent accumulation algorithm for maneuvering target based on IAR-STFT.

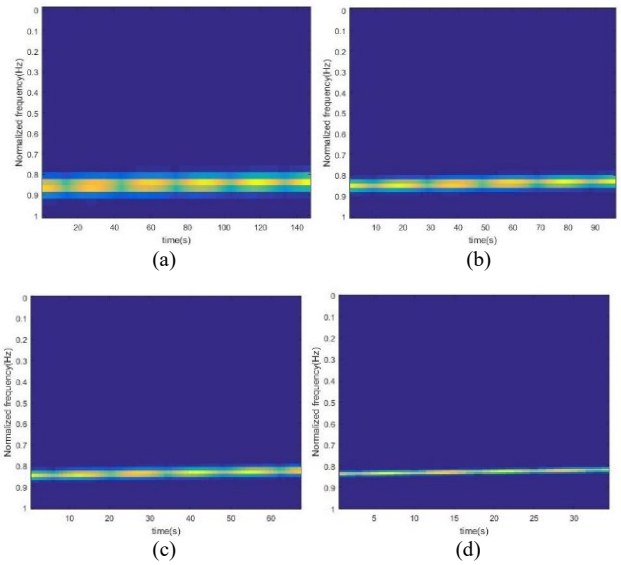

Fig. 4. The two-dimensional resolution maps of several different window widths: (a) $L = 32$, (b) $L = 48$, (c) $L = 66$, (d) $L = 128$.

Initial slant range	200 km
Radial velocity	150 m/s
Radial acceleration	10 m/s^2
SCR(after pulse compression)	–38 dB
Number of window widths	66

Tab. 3. Motion parameters of target.

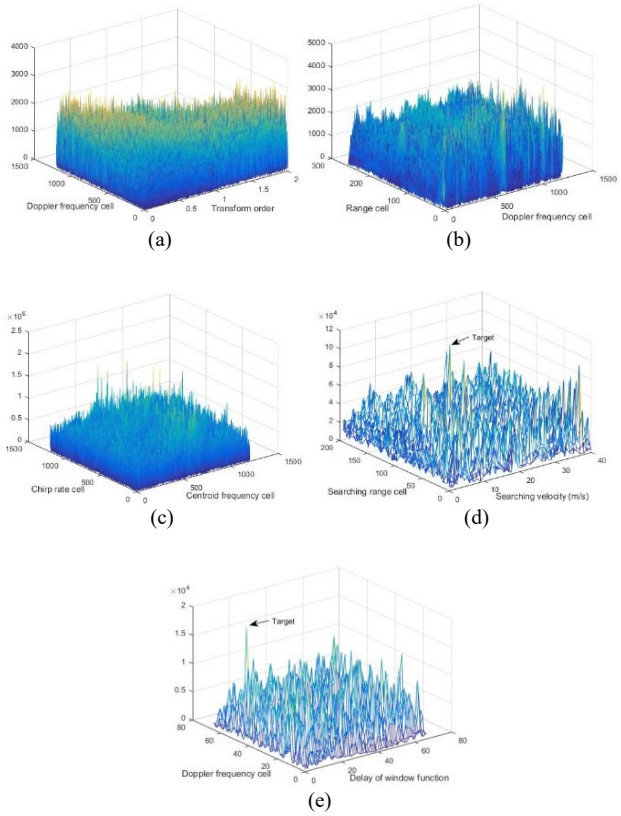

Fig. 5. Coherent accumulation for a weak target via RFRFT, RLVD, GRFT and IAR-STFT: (a) RFRFT, (c) RLVD, (d) GRFT, (e) IAR-STFT.

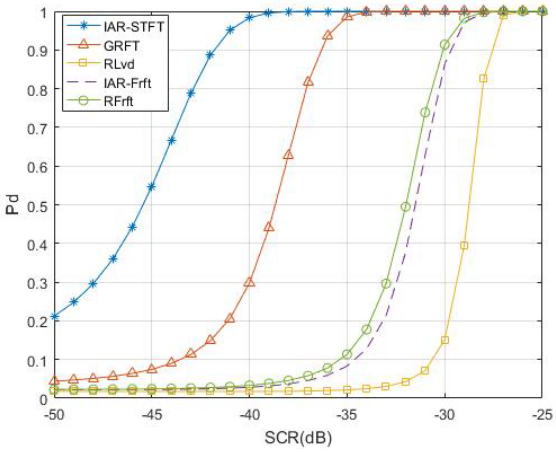

Fig. 6. Detection probability of IAR-STFT, GRFT, RFRFT, IAR-FRFT and RLVD.

4.4 Detection Ability of Different Delays

The detection performance of IAR-STFT algorithm is affected not only by the different window width, but also by the different window delays. When the delay of the window equals the width of window, the signal amplitude decreases for multiplying a Gaussian window, which results in a decline in detection performance. So we can reduce each delay of window appropriately to reuse part of the energy of signal to improve the detection ability. However, this results in the increasing of computational complexity. To get a more optimal delay of window, the detection probability versus different delays of window is given in Fig. 7.

When the delay of the window is smaller than its width, the accumulated energy of the target will alter with the varying overlapping of the window because the target energy in each window is reused. When the ratio of window width to the delay increases, the overlapping part of the window function will also increase, which can improve the accumulated energy of the echoes and the detection probability of target. It can be seen from Fig. 7 that when *n* of WDR is 3, the detection probability is almost 1. The detection probability of target can be improved by increasing WDR. Thus the detection result is more reliable while the SCR is low. Figure 8 shows the experimental results when SCR is –44 dB. According to the results, the detection probability nearly equals 1 when *n* equals 6.

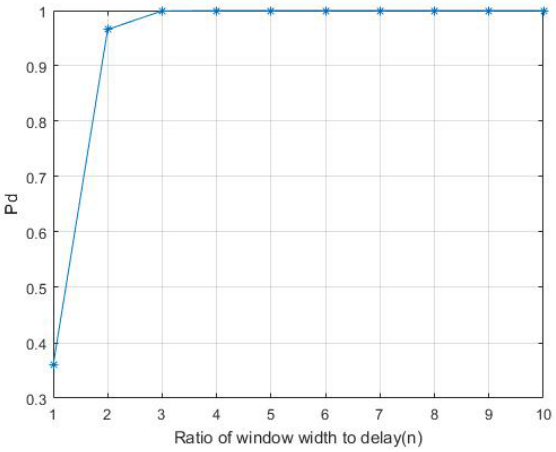

Fig. 7. The detection probability under different delays of window (*SCR* = –38 dB).

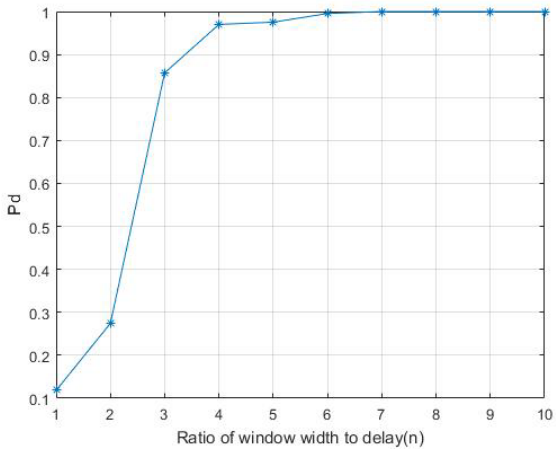

Fig. 8. The detection probability under different delays of window (*SCR* = –44 dB).

4.5 Computational Cost

Suppose that M_t, N_p, N_r, N_v, N_a and K indicate the number of lag samples to RLVD, the number of transform order to RFRFT, the searching number of the initial slant range, the searching number of the equivalent radial velocity, the searching number of the equivalent radial acceleration, and the number of moving times of the window, respectively.

1) IAR-STFT

The computational complexity of this algorithm mainly includes the IAR-STFT of the pulse compression signal, the second phase compensation is carried out, and the energy in each window is accumulated and two-dimensional search of velocity and acceleration. Each group of searching includes L-point FFT for K times, the compensation is a K point matrix multiplication operation, and energy accumulation includes K-point FFT in each range cell. Therefore, the amount of calculation for this algorithm is $O[N_v N_a N_r (KL \log_2 L)(K + K \log_2 K)]$.

2) GRFT [42]

This algorithm removes RM by three-dimensional searching, and the GRFT algorithm cannot directly use the FFT-based filter bank because the input data are different for different filters. This algorithm removes DFM by compensation for each data. Therefore, the amount of calculation for this algorithm is $O[N_v N_a N_r M^2]$.

3) RFRFT [9], [20]

This algorithm removes RM by three-dimensional searching and eliminates DFM by FRFT. The computational load of FRFT is $O[N_p M \log_2 M]$. Therefore, the

amount of calculation is $O[N_{\mathrm{v}}N_{\mathrm{a}}N_{\mathrm{r}}N_{\mathrm{p}}M\log_2 M]$.

4) IAR-FRFT [21]

This algorithm removes RM by searching velocity and eliminates DFM by FRFT for each range cell. Therefore, the amount of calculation is $O[N_{\mathrm{v}}N_{\mathrm{a}}N_{\mathrm{r}}N_{\mathrm{p}}M\log_2 M]$.

5) RLVD [25–27]

This algorithm exploits three-dimensional searching to remove RM. DFM is eliminated by LVD. The computational load of the LVD operation includes the SFT-IFFT interpolation operation $O[4M_{\mathrm{t}}M\log_2 M]$ and two dimensional FFT operation $O[M_{\mathrm{t}}M\log_2 M + M_{\mathrm{t}}M\log_2 M_{\mathrm{t}}]$. Therefore, the amount of calculation for this algorithm is $O[N_{\mathrm{v}}N_{\mathrm{a}}N_{\mathrm{r}}(4M_{\mathrm{t}}M\log_2 M + M_{\mathrm{t}}M\log_2 M + M_{\mathrm{t}}M\log_2 M_{\mathrm{t}})]$.

In the simulations, let $N_{\mathrm{r}}=N$, $M_{\mathrm{t}}=M$, $LK=4M$. The computational complexity comparisons are shown in Tab. 4.

5. Conclusions

Based on the temporal and spatial correlation of sea clutter, this paper adopts a suitable sea clutter model, and proposes a novel algorithm IAR-STFT to detect the weak moving target in the sea clutter. It solves the problem that FFT cannot deal with non-stationary signals. The pulse compression signal is divided into several suitable blocks after eliminating the RM through the IAR, and each block of signals can be regarded as stationary, which can be processed by FFT, and all block signals are accumulated after phase compensating. Finally, the effectiveness of this algorithm is verified by several simulations. The results show that the detection performance of IAR-STFT is superior to that of the RFRFT, IAR-FRFT, GRFT and RLVD, e.g., when the SNR is –45 dB, the detection performance of IAR-STFT is about 55%, which is higher than that of GRFT, RLVD, IAR-FRFT and RFRFT. And by reducing the delay of the window, the detection performance of the IAR-STFT algorithm can be improved in a lower SCR.

Algorithms	Computational complexity
IAR-STFT	$O[NN_{\mathrm{v}}N_{\mathrm{a}}K(KL\log_2 L)(1+\log_2 K)]$
GRFT	$O[NN_{\mathrm{v}}N_{\mathrm{a}}M^2]$
RFRFT	$O[NN_{\mathrm{v}}N_{\mathrm{a}}N_{\mathrm{p}}M\log_2 M]$
IAR-FRFT	$O[NN_{\mathrm{v}}N_{\mathrm{a}}N_{\mathrm{p}}M\log_2 M]$
RLVD	$O[NN_{\mathrm{v}}N_{\mathrm{a}}(6M^2\log_2 M)]$

Tab. 4. Comparison of computational complexity.

Acknowledgments

The authors would like to thank the reviewers for their valuable comments on the paper. This work is supported by the National Nature Science Foundation of China under Grants 62161029 and 62261040, Jiangxi Provincial Natural Science Foundation under Grants 20202BABL202002, 20192BAB207001 and SAST2018078.

References

[1] SIMON, R. A., VINOD KUMAR, P. B. A nonlinear sea clutter analysis using chaotic system. In *2013 Fourth International Conference on Computing, Communications and Networking Technologies (ICCCNT)*. Tiruchengode (India), 2013, p. 1–5. DOI: 10.1109/ICCCNT.2013.6726729

[2] LIU, H. Y., XIONG, W., SONG, J. Analysis of sea clutter characteristics at high grazing angle. In *2017 International Conference on Computer Systems, Electronics and Control (ICCSEC)*. Dalian (China), 2017, p. 216–220. DOI: 10.1109/ICCSEC.2017.8446829

[3] YANG, B. Y., JIANG, M., WANG, J. M. Analysis of extendibility of sea clutter model in high sea states based on measured data. In *2022 3rd International Conference on Computer Vision, Image and Deep Learning & International Conference on Computer Engineering and Applications (CVIDL & ICCEA)*. Changchun (China), 2022, p. 140–143. DOI: 10.1109/CVIDLICCEA56201.2022.9825361

[4] ZHOU, J., CHEN, D., SUN, D. W. K distribution sea clutter modeling and simulation based on ZMNL. In *2015 8th International Conference on Intelligent Computation Technology and Automation (ICICTA)*. Nanchang (China), 2015, p. 506–509. DOI: 10.1109/ICICTA.2015.279

[5] MARIER, L. J. Correlated K-distributed clutter generation for radar detection and track. *IEEE Transactions on Aerospace and Electronic Systems*, 1995, vol. 31, no. 2, p. 568–580. DOI: 10.1109/7.381906

[6] CHEN, X. L., YONG, H., GUAN, J., et al. Sea clutter suppression and moving target detection method based on clutter map cancellation in FRFT domain. In *Proceedings of 2011 IEEE CIE International Conference on Radar*. Chengdu (China), 2011, p. 438–441. DOI: 10.1109/CIE-Radar.2011.6159571

[7] CHEN, X. L., SONG, J., GUAN, J., et al. Moving target detection at sea based on fractal characters in FRFT domain. In *2011 IEEE RadarCon (RADAR)*. Kansas City (MO, USA), 2011, p. 001–005. DOI: 10.1109/RADAR.2011.5960488

[8] HUANG, X., TANG, S. Y., ZHANG, L. R., et al. Low-observable maneuvering target detection based on Radon-advanced discrete chirp Fourier transform. In *2017 IEEE Radar Conference (RadarConf)*. Seattle (WA, USA), 2017, p. 0735–0738. DOI: 10.1109/RADAR.2017.7944300

[9] CHEN, X., JIAN, G., LIU, N., et al. Maneuvering target detection via radon-fractional Fourier transform-based long-time coherent integration. *IEEE Transactions on Signal Processing*, 2014, vol. 62, no. 4, p. 939–953. DOI: 10.1109/TSP.2013.2297682

[10] XU, J., PENG, Y. N., XIA, X. G., et al. Radon-Fourier transform for radar target detection (I): Generalized Doppler filter bank. *IEEE Transactions on Aerospace and Electronic Systems,* 2011, vol. 47, no. 2, p. 1186–1202. DOI: 10.1109/TAES.2011.5751251

[11] XU, J., YU, J., PENG, Y. N., et al. Radon-Fourier transform for radar target detection (II): Blind speed sidelobe suppression. *IEEE Transactions on Aerospace and Electronic Systems,* 2011, vol. 47, no. 4, p. 2473–2489. DOI: 10.1109/TAES.2011.6034645

[12] NI, R., FAN, C. Y., HUANG, X. T., et al. An improved track-before-detection algorithm based on dynamic neighborhood search. In *2017 International Conference on Computing Intelligence and Information System (CIIS)*. Nanjing (China), 2017, p. 150–154. DOI: 10.1109/CIIS.2017.31

[13] BAO, Z. C., JIANG, Q. X., LIU, F. Z. Multiple model efficient particle filter based track-before-detect for maneuvering weak targets. *Journal of Systems Engineering and Electronics*, 2020, vol. 31, no. 4, p. 647–656. DOI: 10.23919/JSEE.2020.000040

[14] TAO, R., ZHANG, N., WANG, Y. C. Analysing and compensating the effects of range and Doppler frequency migrations in linear frequency modulation pulse compression radar. *IET Radar, Sonar & Navigation*, 2011, vol. 5, no. 1, p. 12 to 22. DOI: 10.1049/iet-rsn.2009.0265

[15] SUN, Z., LI, X., CUI, G., et al. A fast approach for detection and parameter estimation of maneuvering target with complex motions in coherent radar system. *IEEE Transactions on Vehicular Technology,* 2021, vol. 70, no. 10, p. 10278–10292. DOI: 10.1109/TVT.2021.3104659

[16] CAO, Y. F., WANG, W. Q., ZHANG, S. Long-time coherent integration for high-order maneuvering target detection via zero-trap line extraction. *IEEE Transactions on Aerospace and Electronic Systems,* 2021, vol. 57, no. 6, p. 4017–4027. DOI: 10.1109/TAES.2021.3082718

[17] ÇULHA, O., TANIK, Y. Low complexity keystone transform and radon Fourier transform utilizing chirp-z transform. *IEEE Access*, 2020, vol. 8, p. 105535–105541. DOI: 10.1109/ACCESS.2020.3000998

[18] LU, Y. F., KASAEIFARD, A., ORUKLU, E., et al. Performance evaluation of fractional Fourier transform (FrFT) for time-frequency analysis of ultrasonic signals in NDE applications. In *2010 IEEE International Ultrasonics Symposium*. San Diego (CA, USA), 2010, p. 2028–2031. DOI: 10.1109/ULTSYM.2010.5935838

[19] CHEN, X. L., CAI, F. Q., CONG, Y., et al. Radon-fractional Fourier transform and its application to radar maneuvering target detection. In *2013 International Conference on Radar*. Adelaide (SA, Australia), 2013, p. 346–350. DOI: 10.1109/RADAR.2013.6652011

[20] GAO, C., TAO, R., KANG, X. J. Weak target detection in the presence of sea clutter using radon-fractional Fourier transform canceller. *IEEE Journal of Selected Topics in Applied Earth Observations and Remote Sensing*, 2021, vol. 14, p. 5818–5830. DOI: 10.1109/JSTARS.2021.3078723

[21] RAO, X., TAO, H. H., SU, J., et al. Detection of constant radial acceleration weak target via IAR-FRFT. *IEEE Transactions on Aerospace and Electronic Systems*, 2015, vol. 51, no. 4, p. 3242 to 3253. DOI: 10.1109/TAES.2015.140739

[22] YU, J., XU, J., PENG, Y. N., et al. Radon-Fourier transform for radar target detection (III): Optimality and fast implementations. *IEEE Transactions on Aerospace and Electronic Systems,* 2012, vol. 48, no. 2, p. 991–1004. DOI: 10.1109/TAES.2012.6178044

[23] ZHANG, Y., XIONG, W., DONG, X. C., et al. Radial accelerated velocity estimation for moving ship target imaging based on GRFT in geosynchronous SAR. In *2019 International Applied Computational Electromagnetics Society Symposium - China (ACES)*. Nanjing (China), 2019, p. 1–2. DOI: 10.23919/ACES48530.2019.9060533

[24] XU, J., ZHOU, X., QIAN, L. C., et al. Hybrid integration for highly maneuvering radar target detection based on generalized radon-Fourier transform. *IEEE Transactions on Aerospace and Electronic Systems,* 2016, vol. 52, no. 5, p. 2554–2561. DOI: 10.1109/TAES.2016.150076

[25] YAO, D. H., ZHANG, X. Y., SUN, Z. B. Long-time coherent integration for maneuvering target based on second-order keystone transform and Lv's distribution. *Electronics*, 2022, vol. 11, no. 13, p. 1–15. DOI: 10.3390/ELECTRONICS11131961

[26] LI, X. L., CUI, G. L., YI, W., et al. Coherent integration for maneuvering target detection based on Radon-Lv's distribution. *IEEE Signal Processing Letters,* 2015, vol. 22, no. 9, p. 1467 to 1471. DOI: 10.1109/LSP.2015.2390777

[27] LV, X. L., BI, G. A., WAN, C. R., et al. Lv's distribution: Principle, implementation, properties, and performance. *IEEE Transactions on Signal Processing*, 2011, vol. 59, no. 8, p. 3576 to 3591. DOI: 10.1109/TSP.2011.2155651

[28] LUO, S., BI, G. A., LV, X. L., et al. Performance analysis on Lv distribution and its applications. *Digital Signal Processing,* 2013, vol. 23, no. 3, p. 797–807. DOI: 10.1016/j.dsp.2012.11.011

[29] RAO, X., TAO, H. H., SU, J., et al. Axis rotation MTD algorithm for weak target detection. *Digital Signal Processing*, 2014, vol. 26, p. 81–86. DOI: 10.1016/j.dsp.2013.12.003

[30] RAO, X., ZHONG, T. T., TAO, H. H., et al. Improved axis rotation MTD algorithm and its analysis. *Multidimensional Systems and Signal Processing,* 2019, vol. 30, no. 2, p. 885–902. DOI: 10.1007/s11045-018-0588-y

[31] KHAN, M. N., HASNAIN, S. K., JAMIL, M., et al. *Electronic Signals and Systems: Analysis, Design and Applications*. 1st ed. River Publishers, 2020, p. 329–343. ISBN: 978-8770221702

[32] ZHANG, X. Q., LIU, R. L. Analysis of linear FM signal based on the STFT in the filtering viewpoint. In *2018 IEEE 3rd International Conference on Signal and Image Processing (ICSIP)*. Shenzhen (China), 2018, p. 389–392. DOI: 10.1109/SIPROCESS.2018.8600426

[33] KIM, B., KONG, S. H., KIM, S. Low computational enhancement of STFT-based parameter estimation. *IEEE Journal of Selected Topics in Signal Processing,* 2015, vol. 9, no. 8, p. 1610–1619. DOI: 10.1109/JSTSP.2015.2465310

[34] YI, L., YAN L., HAN, N. Simulation of inverse Gaussian compound Gaussian distribution sea clutter based on SIRP. In *2014 IEEE Workshop on Advanced Research and Technology in Industry Applications (WARTIA)*. Ottawa (ON, Canada), 2014, p. 1026–1029. DOI: 10.1109/WARTIA.2014.6976451

[35] HU, Y. H., LUO, F., ZHANG, B. B., et al. Simulation of coherent correlation K-distribution sea clutter based on SIRP. In *2006 CIE International Conference on Radar.* Shanghai (China), 2006, p. 1 to 4. DOI: 10.1109/ICR.2006.343185

[36] ZHAO, Y. Q., ZOU, Z. G., WU, L. W., et al. Frequency detection algorithm for frequency diversity signal based on STFT. In *2015 Fifth International Conference on Instrumentation and Measurement, Computer, Communication and Control (IMCCC)*. Qinhuangdao (China), 2015, p. 790–793. DOI: 10.1109/IMCCC.2015.173

[37] FOURER, D., AUGER, F., CZARNECKI, K., et al. Chirp rate and instantaneous frequency estimation: Application to recursive vertical synchrosqueezing. *IEEE Signal Processing Letters*, 2017, vol. 24, no. 11, p. 1724–1728. DOI: 10.1109/LSP.2017.2714578

[38] ZHANG, X. W., ZUO, L., YANG, D. D., et al. Coherent-like integration for PD radar target detection based on short-time Fourier transform. *IET Radar, Sonar & Navigation*, 2020, vol. 14, no. 1, p. 156–166. DOI: 10.1049/iet-rsn.2019.0190

[39] CHEN, T., LIU, L. Z., HUANG, X. S. LPI radar waveform recognition based on multi-branch MWC compressed sampling receiver. *IEEE Access*, 2018, vol. 6, p. 30342–30354. DOI: 10.1109/ACCESS.2018.2845102

[40] TAO, R., LI, Y. L., WANG, Y. Short-time fractional Fourier transform and its applications. *IEEE Transactions on Signal Processing,* 2010, vol. 58, no. 5, p. 2568–2580. DOI: 10.1109/TSP.2009.2028095

[41] HOU, H. L., PANG, C. S., GUO, H. L., et al. Study on high-speed and multi-target detection algorithm based on STFT and FRFT combination. *Optik - International Journal for Light and Electron Optics,* 2015, vol. 127, no. 2, p. 713-717. DOI: 10.1016/j.ijleo.2015.10.140

[42] DURAK, L., ARIKAN, O. Short-time Fourier transform: Two fundamental properties and an optimal implementation. *IEEE Transactions on Signal Processing*, 2003, vol. 51, no. 5, p. 1231 to 1242. DOI: 10.1109/TSP.2003.810293

About the Authors …

Yaowen LIU was born in Shaanxi province, China in 1996. He received the B.Eng. degree in Communication Engineering from the Xi'an University of Posts & Telecommunications, Xi'an, China, in 2020. He is currently pursuing the M.S. degree in Signal Processing from the School of Information Engineering, Nanchang Hangkong University. His current research interests include radar signal processing, radar communication integration and weak detection.

Xuan RAO was born in Jiangxi Province, P.R. China, in 1977. He received the B.Sc. and M.Sc. degrees from the School of Information Engineering, Nanchang University, Nanchang, China, in 1999 and 2005, respectively; and the Ph.D. degrees from the School of Electronic Engineering, Xidian University, Xi'an, China, in 2015. He is currently an Associate Professor of the School of Information Engineering, Nanchang Hangkong University, China. He is a member of IEEE and his current research interests include radar signal processing, weak target detection and tracking.

Jianfen HU (corresponding author) was born in Jiangxi Province, P.R. China, in 1978. She received the Master degree from the School of Measuring and Control Engineering, the Northwestern Polytechnical University, Xi'an, China, in 2005. Her current research interests include signal processing, weak target detection and tracking.

Xiangsheng ZHU was born in Nanchang, Jiangxi, China, in 1993. He received the B.Eng. degree in Electronic and Information Engineering from the Pingxiang University, Pingxiang, China, in 2018. He received the M.S. degree in Signal Processing from the School of Information Engineering, Nanchang Hangkong University, China, in 2021. His current research interests include radar signal processing, weak detection and tracking.

Hong YI was born in Jiangxi Province, P.R. China, in 1977. She received the Master degree in Computer Science from the School of Measuring and Control Engineering, Nanchang Hangkong University, Nanchang, China, in 2006. She is currently a lecturer of the School of Information Engineering, Nanchang Hangkong University, China. Her current research interests include control theory and control engineering.